

Seismic response of a pile-supported excavation on Santiago gravel



G. Pardo, E. Sáez & C. Ledezma

Pontificia Universidad Católica de Chile, College of Engineering, Department of Structural and Geotechnical Engineering, Santiago, Chile

SUMMARY

Non-secant anchored piling support is one of the most frequent earth-retaining systems for temporary deep excavations in Santiago, Chile. The main advantages of using non-secant piling support are their relatively low cost and ease of installation. This system is particularly efficient on stiff soils with deep groundwater table, conditions usually found in Santiago, Chile.

This paper presents the results of a numerical investigation aimed to study the characteristics of earthquake-induced lateral pressures on a recently built pile-supported excavation in Santiago. The estimated static deformations of the piles (including the so-called “arching effect”) were compared against some measurements performed during the excavation.

The dynamic pressures, and their influence on the piles’ internal forces, were evaluated using a synthetic Ricker wavelet in the numerical FE model. These results were then compared against some simplified design recommendations.

Keywords: non-secant anchored piling support, finite element modeling, in-situ measurements, dynamic analysis

1. INTRODUCTION

Discontinuous piling support (non-secant piling support) is one the most frequent forms of retaining systems for temporary deep excavations in Santiago (Figure 1a). The main advantages of using discontinuous piling support are its relatively low cost and ease of installation. The system is particularly efficient in stiff soils with deep water tables, conditions usually found in Santiago, Chile. A proper design of this type of retaining system must prevent its failure and avoid damage to existing nearby structures; the latter is a crucial component of the seismic verification of temporary pile-supported excavations. Unfortunately, there are very few studies concerning the dynamic behavior of pile-supported excavations and earthquake-induced lateral pressures on non-secant piling support. This is partly due to the difficulty of properly including the so-called “arching effect”, which is a 3D phenomenon that controls the mechanical behavior of discontinuous pile-supported excavations. In general terms, this effect consists on the redistribution of stresses from yielding mass of soil to adjacent less-yielding, or restrained, portions of the soil mass.

The phenomenon of “arching” has been recognized for decades, but research on this topic has been sporadic and usually focused on particular problems. Probably, the most familiar application of the vertical arching effect is present in tunnel design. In the field of geotechnical engineering, one of the most important contributions is that of Terzaghi (1943), who explained the phenomenon as the pressure transfer from a yielding mass of soil to adjacent rigid boundaries through the “trap-door test”. This pressure transfer phenomenon was called “arching”. The trapdoor test has been extensively discussed using analytical and numerical methods. For example, Handy (1983) extended the analytical formulation proposed by Terzaghi to the case of retaining walls, with a method that takes into account the relative roughness between the structural element and the surrounding soil. Later, Harrop-Williams (1989) used an analytical approach to propose approximated solutions and improvements concerning

the “arch” shape. More recently, Paik and Salgado (2003) performed an analytical study of the vertical distribution of lateral pressures acting on rigid retaining walls, including arching effects, and they developed some recommendations for vertical distributions of pressures to be used in the design of rigid retaining elements.

Numerical modeling has also been used to evaluate the role of the arching effect on the static lateral pressures. Most of these studies have focused on geotechnical engineering applications of the arching effect that differ from the one presented in this paper. For example, Low et al. (1994) studied the reduction of embankments settlements using piles; Lee et al. (2006) analyzed the role of arching effects during tunneling in soft clayey soil; and Chen and Martin (2002) discussed the resistance mobilization of passive pile groups subjected to lateral soil movement, from the arching-effect point of view.

On the topic of potential benefits of the arching effect on pile-supported excavations, the available literature is very scarce. Vermeer et al. (2001) performed numerical and empirical studies of a wall consisting of anchored steel piles with horizontal timber lagging. They proposed both, two-dimensional and three-dimensional, finite element modeling approaches to reproduce the displacements observed on the field, and their results confirmed the suitability of finite element analyses. Hong et al. (2003) performed a numerical study on the effects of “smearing” the stiffness of soldier piles and timber laggings to construct averaged two-dimensional models to represent three-dimensional situations. Their results were compared against an actual case-study conducted by O’Rourke (1975) with partial success. They found that increasing the inter-pile spacing tends to emphasize the modeling errors obtained with an equivalent plane-strain approach.

Regarding the specific topic of discontinuous pile-supported excavations in Santiago gravel, there is some field data available from an underpinned excavation instrumented in 1982 (Bravo, 1982; Arias, 1984), and recently, some field measurements from an excavation instrumented with inclinometers in Santiago had become available (Tapia, 2011) (Figure 1b). Additionally, some numerical studies have been conducted to study the static arching effects (Medina, 2003; García, 2009). Unfortunately, to the authors’ knowledge, no experimental or numerical studies have been conducted for this problem considering dynamics loads.

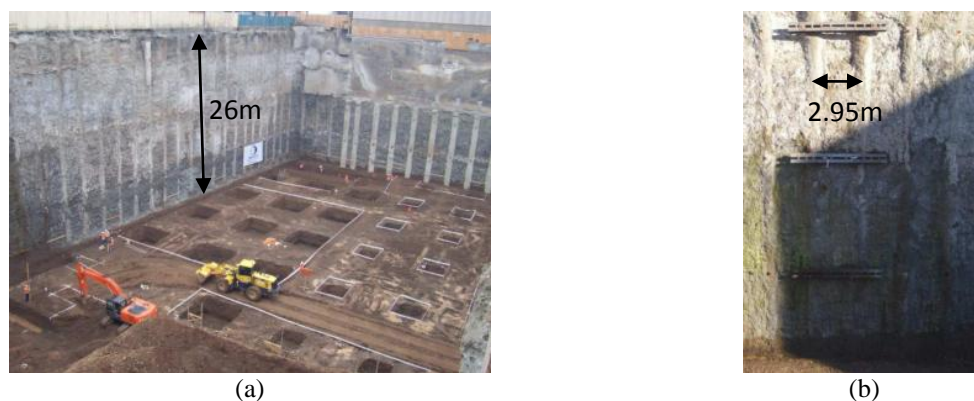


Figure 1. Typical excavation with non-secant anchored piling support, Beauchef building in Santiago, Chile (Tapia, 2011)

The literature review shows that there is still a need for an accurate yet practical procedure for the evaluation of lateral induced pressures on discontinuous pile-supported excavation. Such a procedure will be very useful to improve the current seismic design practice. Even though there is no information concerning failures of this kind of excavation during the Mw8.8 February 27, 2010 earthquake, practitioners are aware that the design approach for this type of excavation support might be overly conservative due to many sources of uncertainties regarding its actual dynamic behavior. Thus, a more precise knowledge of the expected seismic response of these systems could reduce the cost of new projects, without affecting their reliability, and it may improve earthquake-engineering practice.

2. NUMERICAL MODELLING

Several aspects were considered to perform this numerical analysis: (i) selection and calibration of a constitutive model able to reproduce the static and dynamic behavior of Santiago gravel, (ii) geometrical definition of a finite element model suitable for the target problem, (iii) numerical simulation of the excavation sequence, and (iv) earthquake perturbation around the static equilibrium. The specifics for each one of these aspects are detailed in the following sub-sections.

2.1. Selection and Calibration of the Constitutive Model

Santiago gravel is characterized by a fines content of about 3%, with a plastic index between 5 and 20, and coarse grains of up to 30 cm of nominal size (Rodríguez-Roa, 2000). This gravel deposit is usually overlaid by a 1.5–3.0 m thick deposit of low-plasticity clay of medium to high consistency. From the surface down to a depth of 5–7 m, the gravel contains low-plasticity silty fines, with a cohesion of about 20 kPa, and an angle of internal friction as high as 45°. This upper gravelly layer is known as the Second Deposition of the Mapocho River. This stratum is underlaid by the First Deposition of the Mapocho River. The first deposition is denser than the second one, but it has a similar granulometry. The mechanical properties of this material have been studied by many authors (e.g., Kort et al., 1979; Ortigosa et al., 1982; Rodríguez-Roa, 2000; De la Hoz, 2007).

The Ecole Centrale Paris (ECP)'s elasto-plastic multi-mechanism model (Hujeux, 1985) was used to represent the behavior of Santiago gravel. This effective-stress model can take into account the soil behavior in a large range of deformations. The representation of all irreversible phenomena is made by four coupled elementary plastic mechanisms: three plane-strain deviatoric plastic deformation mechanisms in three orthogonal planes, and an isotropic one. The model uses a Coulomb-type failure criterion and the critical-state concept. The evolution of hardening is based on the plastic strain (deviatoric and volumetric strains for the deviatoric mechanisms, and volumetric strain for the isotropic one). A kinematical hardening, based on the state variables at the last load reverse, is used to take into account the cyclic behavior. The soil behavior is decomposed into pseudo-elastic, hysteretic, and mobilized domains.

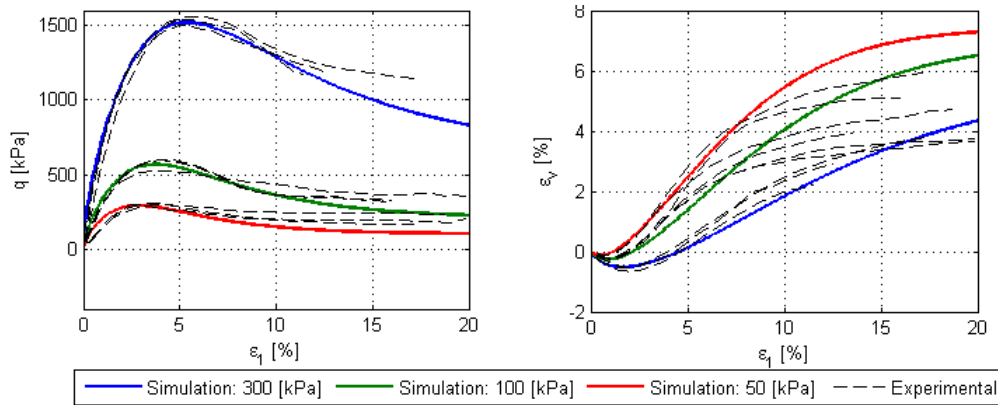


Figure 2. Comparison between simulated and references curves

The calibration of the constitutive model was based on the consolidated drained monotonic triaxial tests (CID) conducted by De la Hoz (2007) for three levels of effective confinement (p'_0): 50, 100, and 300 kPa. The results by De la Hoz were obtained using a large-scale triaxial test and applying the parallel gradation method in three different coarse soils for conventional scale triaxial test. Figures 2a and 2b show a good agreement between the simulated triaxial paths and the experimental data from De la Hoz.

The referential shear modulus for the model at a mean effective stress of 1 MPa was calculated using the Seed et al. (1986) equation:

$$G_{max} \left[\frac{lb}{ft^2} \right] = 1000 \cdot K_2 \cdot \sqrt{P_o}$$

where G_{max} is the shear modulus; P_o is the mean effective stress in lb/ft^2 and K_2 is a coefficient that depends on the material density. Typical values for this parameter are $K_2 = 30$ for loose sands, $K_2 = 75$ for very dense sands, and $K_2 = 80$ to 180 for relatively dense gravels.

Geophysical measurements, using active and passive techniques, were conducted in an area close to the excavation under study. When the results of these measurements are compared against the values estimated using the previous equation assuming a geostatic stress state, there is not a good agreement for depths of ~ 8 m or larger (Figure 3a). These differences could be related to non-geostatic *in-situ* stresses, to uncertainties in the inversion process used for the geophysical exploration, or simply to the fact that the expression proposed by Seed et al. (1986) might be not directly applicable to Santiago gravel. This specific topic is out of the scope of the present paper, but it will be studied in more detail in future stages of this research. For this study we adopted the shear wave velocity profile shown in red in Figure 3a.

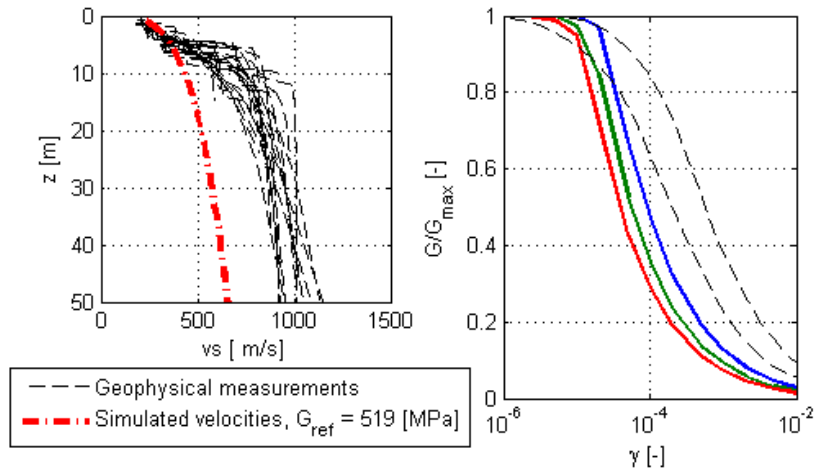


Figure 3. (a) Comparison between simulation and geophysical measurements (b) Comparison between simulation and reference curves for gravel (Seed et al., 1986)

To evaluate the cyclic response using the calibrated parameters for the constitutive model, three cyclic shear tests were simulated using the same three levels of confinement that were used for the drained triaxial tests. The simulated shear modulus degradation and damping curves were compared against the gravel reference curves given by Seed et al. (1986). As Figure 3b shows, the constitutive model produces degradation curves that are comparable to those from the literature, but with a more pronounced stiffness decrease at midlevels of shear strain.

2.2. Finite Element Model and Numerical Simulation

To reproduce the different excavation phases, and to estimate the dynamically-induced lateral pressures on the supporting piles, the temporary excavation under study was modeled as a 3D vertical “slice” which includes two adjacent half-piles and the soil in between (Figure 4).

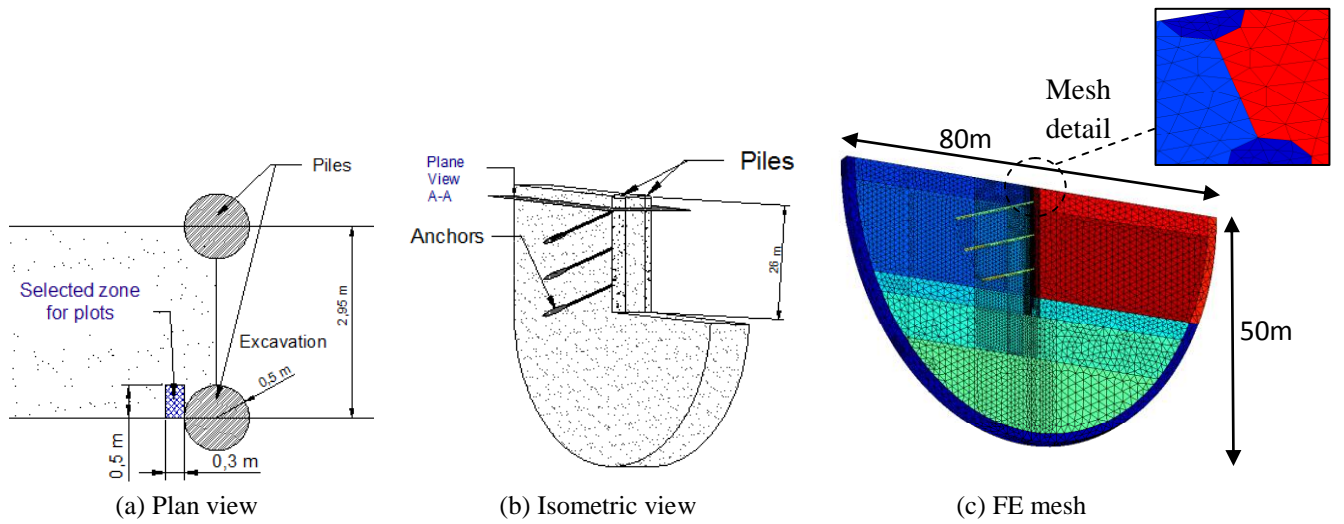


Figure 4. Geometry of the FE model

A hypothetical elastic bedrock 5 m wide and 50 m deep was assumed. In the static part of the problem its influence in terms of stresses and displacements must be negligible. In the dynamic part of the analysis, the objective is to ensure that the wave diffraction induced by the excavation vanishes inside the model, before reaching its lateral boundaries. Since the complete model is inelastic, lateral absorption elements cannot be directly connected to the inelastic soil elements because they require local elastic conditions. To solve this issue, the hypothetic elastic rock was extended to the surface forming, approximately, a half-ellipse. The size of this half-ellipse was selected iteratively in order to obtain a satisfactory free-field condition far enough from the excavation. The input dynamic motion recorded at the outcrop was deconvoluted and imposed at the bedrock. Reflected and diffracted waves at the boundary of the model were absorbed by paraxial-type consistent elements (Modaressi and Benzenati, 1994).

Solid elements were used to represent the soil, the excavated material, and the hypothetic bedrock. The size of the elements was selected to guarantee at least 8 elements per wave-length assuming a cutoff frequency of 15 Hz. The piles were also modeled using solid elements. The relative displacement between the piles and the soil was allowed by interface element obeying a regularized Coulomb frictional criterion. Anchor elements were modeled as one-dimensional bar elements, using a refined meshing in the grout zone in order to improve the stress transfer between the structural element and the surrounding soil.

All computations were conducted using *GEFDyn* finite element code (Aubry and Modaressi, 1996) using an explicit/implicit operator splitting in transient computations, associated to a Newmark numerical scheme. Some numerical dissipation is employed to prevent spurious frequencies and to introduce some damping at very low amplitude. In each step, the inelastic problem is solved using a Newton-Raphson iterative procedure. The complete model has about 115000 tetrahedral elements and more than 25000 nodes (Figure 5c). A very fine mesh was used between the piles in order to properly capture the “arching effect”. Red elements in Figure 5c are progressively removed during the static phase of the computation, to reproduce the sequential excavation process.

3. NUMERICAL RESULTS

Computing time is a critical issue in numerical modeling of dynamic problems. Consequently, to reduce computing time, and as the first part of an ongoing research program, we decided to use synthetic signals (Ricker wavelets).






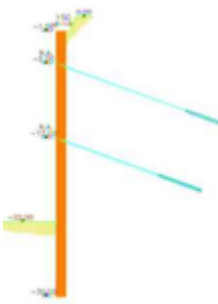
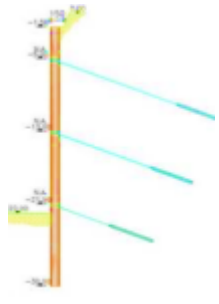
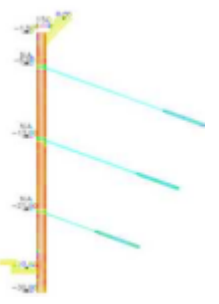
Each numerical computation was composed of two main phases: (1) initialization and simulation of the excavation sequence; and (2) seismic analysis, modeled as a dynamic perturbation around the static state computed in the previous phase. The first phase is modeled using a parametric Lagrangian transformation of the domain in terms of the vertical coordinates of different zones of the model (Aubry and Modaressi, 1989). Hence, the extraction or the addition of material is modeled as a

continuum deformation resulting from the initial configuration. The second phase is performed around the stress state, and hardening internal variables of the constitutive model, computed at the end of the excavation simulation. Usually, a time step of 0.001 s is used to prevent numerical dispersion of consistent boundary elements which are explicitly integrated; however, a 10 times smaller time step was required in this case, because some numerical instabilities were found during the calibration of the dynamic model, which were due to wave reflections close to the free surfaces.

3.1. Sequential excavation

The static phase was modeled using 11 steps describing the installation of the piles, and the sequential excavation and anchors installation. Each step was computed considering long-term conditions, thus creep effects were neglected. The main stages of the construction sequence are shown in Table 1.

Table 1. Main stages of the excavation process

			
Stage 1	Stage 2	Stage 3	Stage 4
			
Stage 5	Stage 6	Stage 7	Stage 8

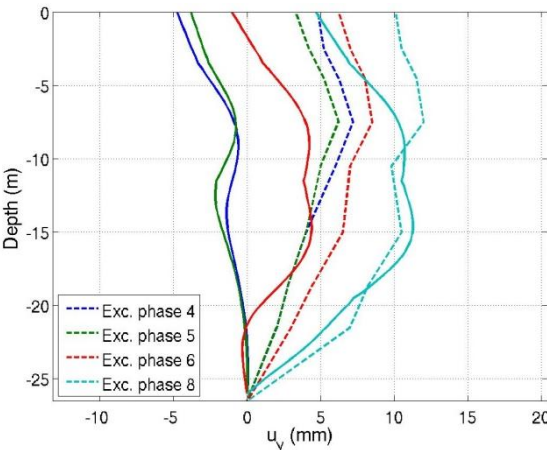


Figure 5. Measured versus simulated lateral displacement profiles of the piles

Figure 5 shows a comparison between the actual lateral displacements of the piles (measured using inclinometers), and the values that were calculated using the finite element model. In this figure, the dashed lines represent measurements and the continuous lines represent computed values. A good

agreement was found at the end of the excavation process (Exc. phase 8 in Figure 5); nevertheless, some important differences were observed during the first stages of the excavation. Unfortunately, the force in the anchors was available only for the initial state and not for the final condition (Tapia, 2011), thus no verification could be performed in this sense. The authors believe that the measured initial and intermediate lateral displacements profiles, especially at early stages of the excavation (stages 4 and 5), could suffer from some misinterpretation since piles deflections in these stages seem unconvincing. In any case, the final displacement profile is properly reproduced by the numerical model, which means that FE model, with the material calibration described in Section 2.1, was able to properly reproduce the key aspects of the problem.

To highlight the ability of the numerical model to reproduce the arching effect in the soil, the stress distribution on a horizontal section of the model was studied. Figure 7a shows this distribution for a cross section at a depth of 5 m ($z=-5$), which is the same as Plan-View AA in Figure 4b. The length of the lines in Figure 6a is proportional to the principal stress value. This figure shows that the soil between piles and close to the free surface (excavation) is almost fully unloaded. Away from the free border, but still close to the piles, the major principal stresses get larger and rotate as to form an “arch” between the piles. Far enough from the piles (approximately at a distance of three times the pile diameter), the arching effect vanishes, and the principal stresses align with the horizontal directions (x and y). Figure 6a also shows that rotation of the principal stresses close to the piles, due to the arching effect, tends to increase the horizontal stresses compared to the geostatic values.

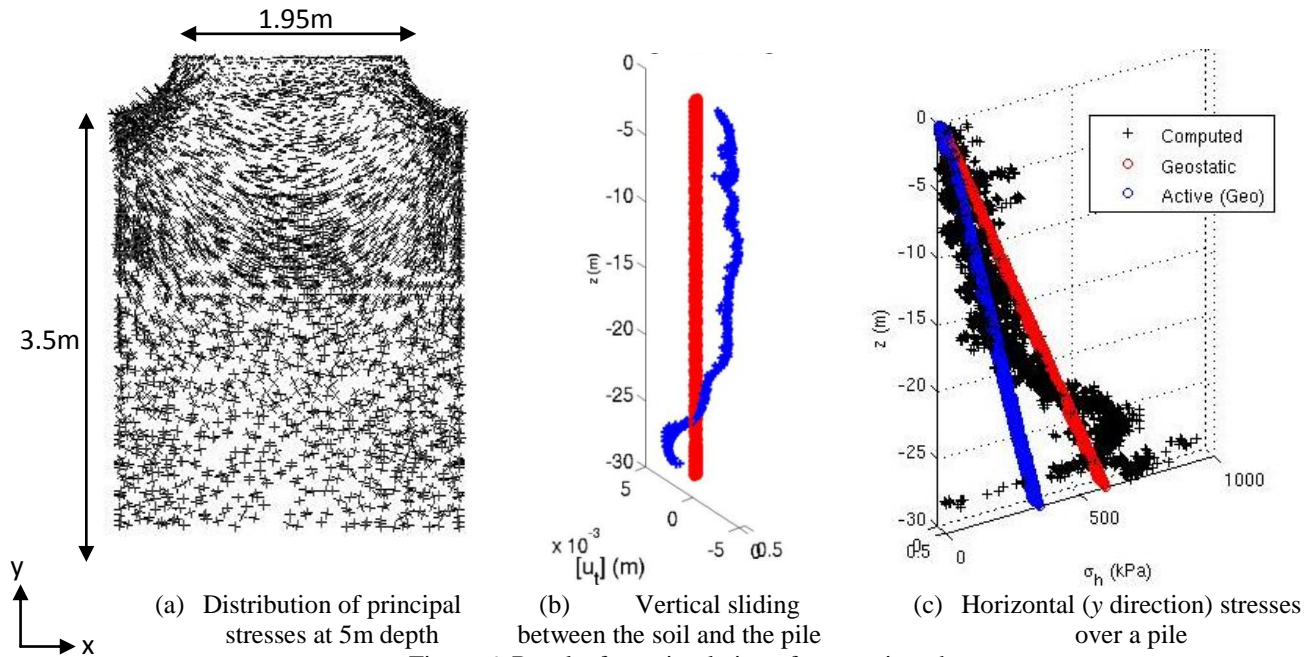


Figure 6. Results from simulation of excavation phase

Figure 6b shows the calculated relative vertical displacement between pile and soil at the interface elements. Negative values correspond to the soil settling with respect to the pile. As expected, the soil behind the piles settles with respect to the piles, and that settlement is about 3 mm. This relative displacement is essentially uniform up to 20 m deep. Below this level, the value gradually goes to zero close to the excavation grade ($z=-26$). Below the excavation grade, the relative vertical displacement becomes positive and the pile settles with respect to the soil. Indeed, below the excavation grade, the soil has significantly reduced its initial confinement, due to the large volume of excavated soil. This strong reduction of vertical load induces an expansion of the soil, which explains the change of sign of the relative settlements.

Representation of the soil pressures that act on the piles is difficult because the pile/soil interface is curved (variable normal direction) and the horizontal stresses are rotated due to the arching effect. Additionally, as automatic mesh tools have been used to construct the FE mesh, element distribution is

not perfectly regular, which means that the integration points are not exactly located in the same horizontal or vertical plane. To solve this issue, we selected a small region of soil behind the piles (Figure 4a) to represent computed pressures that could be compared against reference stress profiles used in traditional design. Figure 6c shows the horizontal stresses (σ_{yy}) retrieved at all integration points in the described region for depths between 0 and 30 m. As a reference, the standard geostatic value assuming a value of $K_0=0.29$ (Jaky's formula) and the corresponding active pressures according to Rankine's theory, are also included in Figure 6c. As expected, the computed values of σ_{yy} are somewhere between the geostatic and the active condition. Nevertheless, in the upper part of the excavation (close to $z = -5$ m), exceptionally large values were obtained. The authors believe that these high values are related to the development of the arching effect, as depicted in Figure 6a. Additionally, in this zone there is a post-stressed anchor, which certainly affects the stress distribution. Below the excavation grade ($z < -26$ m), a second increase of tension can be noticed. As highlighted in the relative vertical sliding distribution (Figure 6b), the soil expands in this zone, which is likely the main cause of this horizontal stress increase. At the bottom of the pile, large stress increases and reductions can be noticed, probably due to the stress concentration that takes place in this zone. Finally, in a rather limited zone close to the bottom of the pile, the horizontal stress falls below the active condition, which is a clear sign that some large shear forces are developing in that zone.

3.2. Dynamic Analysis

To evaluate the dynamic behavior of the pile-supported excavation, an analytic Ricker wavelet with a peak time of 0.8 s, a pseudo-period of 0.2 s, and an amplitude of 0.1g, was selected. Figure 7 displays the Ricker signal and the corresponding Fourier amplitude. The Fourier spectrum shows that the wavelet delivers energy up to 12 Hz, compatible with the typical frequency content of earthquake ground motions recorder on rock. The input motion is imposed by the paraxial elements after deconvolution from a control point placed on the hypothetical outcrop rock. As mentioned previously, this motion was selected to reduce computing time considering the large size of the FE model. Actual recorded ground motions will be used in future stages of this research.

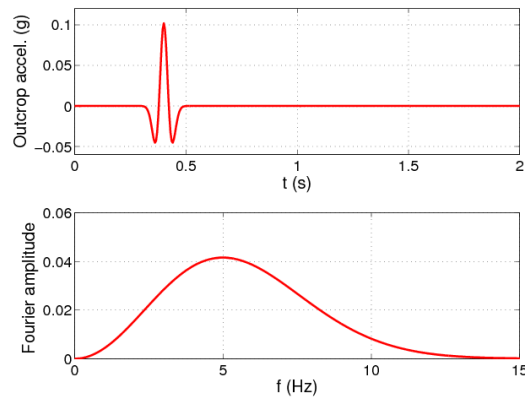


Figure 7. Ricker signal

Unfortunately, during the dynamic analysis soil “detachment” was observed. This phenomenon corresponds to a strong concentration of soil dilation in some regions between piles; more precisely, in the portion of soil close to free-face of the excavation where compressive stresses are very low (Figure 6a). From a numerical point of view, the software is unable to integrate the constitutive model for such large concentration of volumetric strains, and the computation stops. This concentration of deformations is illustrated in Figure 8a, which corresponds to the last computed step for the Ricker wavelet. In this case, a maximum dilation of more than 700% was obtained before the computation stopped, immediately after the strongest part of the ground motion was over. This soil detachment does not necessarily correspond to excavation failure, but it could be interpreted as a local failure of the soil mass, which justifies the use of shotcrete in this type of excavations to prevent these blocks of soil from falling. Soil “detachment” could be very dangerous for operators working in the excavation.

The strain concentrations described in the previous paragraph are accompanied by an abnormal increase of the stresses in the soil in that area. Figure 8b shows the increment of the horizontal stresses due to dynamic effects ($\Delta\sigma_{yy}$) right before the computation stops. It can be noticed that where plastic strains concentrate, i.e., at 4.5 m and 12 m deep, $\Delta\sigma_{yy}$ becomes unrealistically large, indeed ten times larger than the recommendation from the Chilean seismic design code (NCh433Of96Mod2008, 1996) shown in blue in Figure 8b. These high-strain zones coincide, approximately, with the location of the anchors heads, which means that this strain concentration could be related to or triggered by the additional stiffness and/or stress induced by the anchors in these zones.

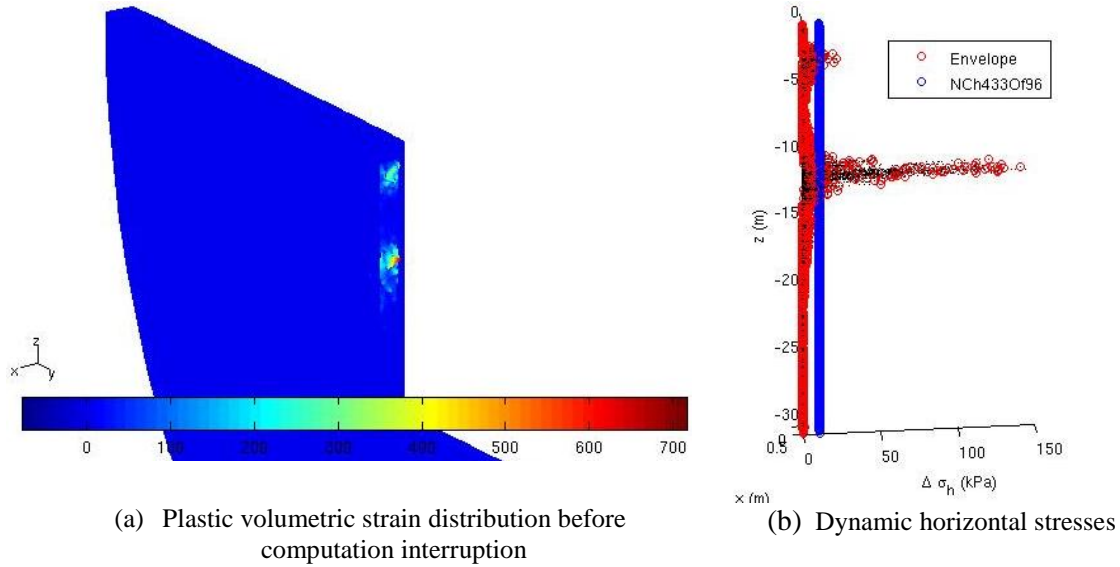


Figure 8. Dynamic analyses' results, illustrating deformation concentration

Due to the three dimensional nature of the arching stress distribution, this effect cannot be included in standard 2D plane-strain models, commonly used in practice. Nevertheless, the dynamical modeling poses new challenges related to local strain concentrations in the free surface of poorly confined dilative material. Several modeling strategies are currently being tested to solve this issue and to obtain a realistic representation of the seismic behavior of this kind of pile-supported excavations.

4. CONCLUSIONS

This paper presents a numerical investigation on the static and dynamic behavior a pile-supported excavation on Santiago gravel.

A successful 3D model was developed for the static phase of the problem, where sequential excavation and anchoring installation were properly simulated. A satisfactory agreement with some in-situ measurements was obtained, in particular with the final profile of horizontal displacements on the piles. The model was able to properly reproduce the stress distribution due to the “arching effect”, and a discussion regarding the vertical stress distributions typically used for design has been included.

During the dynamic modeling phase, a strong strain concentration took place in the soil between the piles at depths that were close to the anchors heads, inducing an unrealistic dynamic response. The numerical modeling of the seismic part of the problem has several challenges that the authors will solve in future stages of this research program.

ACKNOWLEDGEMENT

This work was made possible by a grant from the Chilean National Commission for Scientific and Technological Research under FONDECYT Award Number 11100157.

REFERENCES

- Arias, J.S. (1984). Socializados de Edificios en la Grava de Santiago. Comparación entre Esfuerzos de Diseño y los Medidos en Terreno. *Memoria de Título*, Departamento de Ingeniería Civil, Universidad de Chile (in Spanish).
- Aubry, D. and Modaressi, A. (1989). A rational approach to the analysis of construction filling or excavation. *Proceedings of Numerical Models in Geomechanics*, NUMOG III: 455–462.
- Aubry, D. and Modaressi (1996). A. *GEFDyn: Manuel Scientifique*, Ecole Centrale Paris, France (in French)
- Bravo, C.G. (1982). Mediciones de Esfuerzos en Socializados de Edificios. *Memoria de Título*, Departamento de Ingeniería Civil, Universidad de Chile (in Spanish).
- Chen, C.Y., Martin, G.R. (2002). Soil-structure interaction for landslide stabilizing piles. *Computers and Geotechnics*, Vol. 29, No. 5: 363–386.
- De La Hoz, K. (2007). Estimación de los parámetros de resistencia al corte en suelos granulares gruesos. *Tesis de Magister en Ciencias de la Ingeniería*, Universidad de Chile (in Spanish).
- García, J.M. (2009). Análisis 3D no lineal mediante elementos finitos del efecto arco en la grava de Santiago. *Memoria de Título, Departamento de Ingeniería Estructural y Geotécnica*, Pontificia Universidad Católica de Chile (in Spanish).
- Handy, R.L.(1983). The arch in soil arching. *Journal of Geotechnical Engineering*, ASCE, Vol. 111, No. 3: 302-320.
- Harrop-Williams, K. (1989). Arch in soil arching. *Journal of Geotechnical Engineering*, ASCE, Vol. 115, No. 3: 415-419.
- Hong, S.H., Lee, F.H., Yong, K.Y. (2003). Three-dimensional pile-soil interaction in soldier-piled excavations. *Computer and Geotechnics*, Vol. 30, No. 1: 81-107.
- Hujeux, J.-C. (1985). Une loi de comportement pour le chargement cyclique des sols. *Génie Parasismique*, Presse ENPC: 287-302 (in French).
- Instituto Nacional de Normalización. NCh 433.Of96 (2006). *Diseño sísmico de Edificios, Norma Chilena Oficial* (in spanish).
- Kort, I., Musante, H., and Fahrenkrog, C. In situ mechanical properties measurements of gravelly soil used in an interaction and foundation model for the Santiago Metro. *Proceedings of the 6th Panamerican Conference on Soil Mechanics and Foundation Engineering*, Perú, 217-224, 1979.
- Lee, C.J., Wu, B.R., Chen, H.T., Chiang, K.H. (2006). Tunnel stability and arching effects during tunneling in soft clayey soil. *Tunnelling and Underground Space Technology*, Vol. 21, No. 2: 119-132.
- Lopez-Caballero, F., Modaressi, A. and Modaressi, H. (2007) Nonlinear numerical method for earthquake site response analysis: I- elastoplastic cyclic model & parameter identification strategy. *Bulletin of Earthquake Engineering*, Vol. 5, No. 3: 303-323.
- Low, B.K., Tang, S.K., Choa, V. (1994). Arching in piled embankments. *Journal of Geotechnical Engineering*, ASCE, Vol. 120, No. 11: 1917-1937.
- Medina, C.L. (2003). Estudio del Efecto de Arco. Aplicación a Problemas de Ingeniería Geotécnica. *Memoria de Título*, Departamento de Ingeniería Civil, Universidad de Chile (in Spanish).
- Modaressi, H. and Benzenati, I. (1994). Paraxial approximation for poroelastic media. *Soil Dynamics and Earthquake Engineering*, Vol. 13, No 2: 117-129.
- O'Rourke, T.D. (1975). A study of two braced excavations in sands and interbedded stiff clay. *PhD. Thesis*, University of Illinois.
- Ortigosa, P., Musante, H. and Kort, I. Propiedades mecánicas de la grava de Santiago. *1° Congreso Chileno de Ingeniería Geotécnica*, Santiago: 442-54, 1982 (in spanish).
- Ortigosa, P. (2004), Empujes sísmicos para el diseño de Entibaciones en Grava de Santiago, *Personal communication* (in spanish).
- Paik, K, Salgado, R.(2003). Estimation of Active Earth Pressure Against Rigid Retaining Walls Considering Arching Effects. *Géotechnique*, Vol. 53, No. 7:643-653.
- Rodríguez-Roa, F. (2000). Observed and calculated load-settlement relationship in a sandy gravel. *Canadian Geotechnical Journal*, Vol. 37, No. 2, pp. 333-342.
- Seed, H. B., Wong, R. T., Idriss, I. M., & Tokimatsu, K. (1984). Moduli and damping factors for dynamic analyses of cohesionless soils. *Earthquake Engineering Research Center*, Vol. 112, No 11.
- Terzaghi, K. (1943). Theoretical Soil Mechanics. John Wiley and Sons.
- Vermeer, P.A., Punlor, A., Ruse, N. (2001). Arching effects behind a soldier pile wall, *Computers and Geotechnics*, Vol. 28, No. 6-7: 379–396.